

Research Article

Application of Flax (*Linum Usitatissimum* L.) Straw Derived Activated Carbon Using Phosphoric Acid (H₃PO₄) for the Removal of Nitrate (NO₃⁻) Ions from Aqueous Solutions

Damenech Tefera Werku^{1,*} , Getahun Yifru Desta¹ , Tayto Mindahun² 

¹Department of Chemical Engineering, Debre Berhan University, Debre Berhan, Ethiopia

²Department of Chemical Engineering, Addis Ababa Science and Technology University, Addis Ababa, Ethiopia

Abstract

Significant health and environmental hazards are associated with nitrate (NO₃⁻) contamination in water, which calls for economical and environmentally friendly treatment techniques. This study investigates using phosphoric acid (H₃PO₄) activation to turn flax straw (*Linum usitatissimum* L.), an underutilized agricultural residue, into activated carbon (FS-AC) for the removal of nitrate from aqueous solutions. The FS-AC was prepared by chemical activation under varying conditions (temperature: 400-600 °C, H₃PO₄ concentration: 1-3 M, impregnation ratio: 1:4-1:6) and optimized using response surface methodology (RSM). Characterization via Scanning Electron Microscopy (SEM) revealed a highly porous morphology (surface area: 798.23 m²/g), while X-ray Diffraction (XRD) and Fourier Transform Infrared Spectroscopy (FTIR) confirmed an amorphous carbon structure with oxygen-rich functional groups and residual crystalline phases. Under optimal conditions (532 °C, 1 M H₃PO₄, impregnation ratio 1:5), FS-AC achieved 92.79% nitrate removal at pH 4, 0.25 g/L dose, and 60 min contact time. Adsorption followed the Langmuir isotherm (R²=0.9895), indicating monolayer adsorption, and pseudo-second-order kinetics (R²=0.9408), suggesting chemisorption. Thermodynamic analysis revealed spontaneity (ΔG°: -1.27 to -0.18 kJ/mol) and exothermicity (ΔH°=-14.19 kJ/mol). Generally, the study highlights FS-AC's competitive performance against biomass-derived carbons, with fixed carbon content up to 34.89%. By converting flax straw waste into an efficient adsorbent, this study addresses dual challenges of agricultural residue management and water pollution, aligning with circular economy principles. Thus, future research should explore scalability, regeneration, and application in real wastewater systems to further validate its industrial viability.

Keywords

Adsorption Isotherms, Flax Straw, Nitrate Removal, Phosphoric Acid Activation

1. Introduction

Water pollution is a chronic global issue, with nitrogenous compounds, particularly nitrate (NO₃⁻) being a significant health and environmental risk [1]. Nitrates from agricultural

runoff, industrial effluent, and also wastewater effluent induce eutrophication and toxicity in aquatic organisms. Human exposure is linked with severe health impacts, in-

*Corresponding author: teferadamenech@gmail.com (Damenech Tefera Werku)

Received: 22 March 2025; **Accepted:** 10 April 2025; **Published:** 29 April 2025



Copyright: © The Author(s), 2025. Published by Science Publishing Group. This is an **Open Access** article, distributed under the terms of the Creative Commons Attribution 4.0 License (<http://creativecommons.org/licenses/by/4.0/>), which permits unrestricted use, distribution and reproduction in any medium, provided the original work is properly cited.

cluding methemoglobinemia and carcinogenic nitrosamine formation [2]. Regulatory limits, such as by World Health Organization (WHO) with 3 mg/L, emphasize the necessity of adequate remediation strategies to wastewater treatment [3]. Conventional methods of eliminating nitrate, such ion exchange, reverse osmosis, and biological denitrification, have drawbacks of their own, including high operating costs, high energy requirements, and potential for further pollution problems [4]. While biological methods are cheaper, they are slow and easily affected by the environmental conditions [5].

However, adsorption seems like a good option because it is cheap, pretty simple to set up, and easy for operation [6]. Adsorption of nitrates from wastewater can be performed by using activate carbon. Due to its high surface area and porous structure, activated carbon (AC) is well known for its excellent adsorption capacity [7]. As early as the 18th century, it was noted that the sugar industry could benefit from the highly decolorizing capacity of charcoal with respect to some liquids. It gained activity in 1920, and large-scale production of AC steadily grew and gained popularity, being one of the most useful and versatile adsorbent material till today. Owing to its low cost and unusual properties, such as high specific porosity, high surface area, high adsorption capacity, pore structure, and surface functionalization, AC has been extensively investigated by researchers [8]. As a result, this transition facilitates waste minimization and lowers the dependence on non-renewable sector precursors, and thereby increases sustainability [7].

Flax (*Linum usitatissimum* L.) is an annual plant grown mainly in a temperate region and has great potential to contribute towards the Ethiopian agricultural sector. In Ethiopia, the flax-straw residue from agriculture is very abundant than some other species of plants are grown for energy purposes. Industrial utilization of this flax straw has been neglected and the residue is frequently lost as waste while in Agriculture [9]. The high cellulose and lignin content of flax straw make it a good feedstock for AC preparation as well as dealing with waste management issues [10]. While past research points to its use for bioenergy [10], composite materials [11] and paper and pulp production [9], yet its application in AC remains underexplored.

Recent work shows that AC from farm waste could be good for cleaning up wastewater, with precursors such as for example rice husks [12], sugarcane bagasse [13] and teff straw [14], demonstrating notable adsorption capacities for nitrogenous pollutants also. Activated carbon can be prepared using two basic methods; physical activation and chemical activation. Physical activation involves carbonizing the raw material under heat, followed by activating with steam or CO₂ to create porosity. Chemical activation uses low-temperature chemical reagents, such as potassium hydroxide or phosphoric acid, to form pore structure [15]. Choice of activation procedure plays a key part in establishing the physicochemical properties of produced activated carbon. Phosphoric acid

(H₃PO₄) chemical activation, has attracted great interest attributed to its capability of producing mesoporous structures and rich surface oxygen functional groups that improve anionic adsorption efficiencies [16]. Furthermore, H₃PO₄ is preferred for AC synthesis because it is less corrosive than ZnCl₂ or KOH, promotes oxygen-rich surface groups, and has lower activation temperatures and less of an adverse effect on the environment [14].

Several studies were performed previously with regarding to the application of AC in wastewater treatment. For instance the study by preparation of activated carbon from various agricultural wastes, including rice husks [17], coconut shells [18], corn cobs [19], mixed coconut endocarp and rice husk [20], teff straw [14] and Walnut Waste [21]. There have been, however little literature data with respect to the application of flax straw as a precursor material and especially in support of phosphoric acid activation for nitrate removal from wastewaters. Furthermore, several factors can affect the adsorption properties of activated carbon such as temperature impregnation ratio H₃PO₄ concentration and time [14]. Thus, those factors provide the common mechanisms for all materials to alter important properties of pore structure (pore development), surface functionalization and yield that affect adsorption performance directly [22]. Response surface methodology (RSM) has proven effective in optimizing such parameters for maximal contaminant removal [14].

Therefore, in this study, activated carbon from flax straw was prepared by impregnating it with H₃PO₄ to fill the aforementioned gap and utilized to remove nitrate ions from wastewater. Optimized through a central composite design based on a response surface approach, it offers a novel method for producing highly effective activated carbon for the removal of nitrate ions. It was investigated in relation to calcination at elevated temperatures, impregnation ratio, and H₃PO₄ concentration. The adsorption data was fitted to kinetics and isotherm models, and the impacts of adsorption parameters such as solution pH, initial nitrate concentration, adsorbent dose, and contact time were also investigated. Thermodynamic models further affirmed the feasibility of the process, marking a promising approach in water treatment technologies.

2. Materials and Methods

2.1. Materials and Chemicals

Waste flax straw (*Bekoji-14*) was collected from the Holeta Agricultural Research Center, Ethiopia. Sodium hydroxide (98.5%), hydrochloric acid (37%), and phosphoric acid (85%) were obtained from Sigma Aldrich. All chemicals used in the research were analytical grade.

2.2. Activated Carbon Preparation

2.2.1. Flax Straw Sample Preparation

The harvested flax straw was manually sorted to remove impurities such as dirt, grass, sand, leaves, and other materials that were not required. It was then chopped into pieces using a knife and other tools and thoroughly washed to eliminate dust and remaining impurities. The washed flax straw was left under the sun for five days to remove the moisture before crushing using a high-speed multi-functional grinder. The ground material was also sieved to have a consistent particle size of 125 μm .

2.2.2. Flax Straw Activated Carbon (FS-AC) Preparation

Activated carbon preparation was carried out using previously reported procedures such as by Shewatatek et al. [14] and Neme and Gonfa [23] with some modifications. Accordingly, the flax straw powder having particle size of 125 μm was impregnated with phosphoric acid (H_3PO_4) with

various concentrations (1, 2, and 3 M) for 24 h. To guarantee adequate mixing, FS powder was added to H_3PO_4 and the mixes were vigorously agitated. The weight ratios of H_3PO_4 to flax straw powder for the impregnation were 1:4, 1:5, and 1:6. The impregnated samples were sun-dried and then activated in a muffle furnace with a nitrogen environment for 2 h at three distinct temperatures (400, 500, and 600°C). In this study, the concentration range of 1-3 M was selected based on previously reported literature [1, 2], indicating optimal activation of lignocellulosic materials within this range, promoting efficient impregnation without excessive degradation. Similarly, the temperature range of 400-600 °C was chosen as it is commonly used for thermal activation, allowing for sufficient decomposition of volatile components while preserving carbon yield and enhancing pore structure. After activation with muffle furnace, the activated carbon was cooled to room temperature, washed with 1 M NaOH, and distilled water until the pH of the effluent became 7.0. The cleaned activated carbon was dried at 100 °C for 12 hours and stored for further experimental analysis. The basic steps of activated carbon preparation from flax straw is shown in Figure 1.



Figure 1. Basic steps for the preparation of activated carbon from flax straw.

2.3. Characterizations

The proximate analysis values such as moisture content (MC), volatile matter content (VM), ash content (AC), and fixed carbon content (FC) were determined by employing standard procedures which are presented below. ASTM standard E1756 - 08 was used to ascertain the moisture content of the samples [24]. The moisture content was calculated by using the Eq. 2.

$$MC(\%) = \frac{w_i - w_f}{w_i} \quad (1)$$

The ash content of the samples was determined by using ASTM E1755 - 01 [25]. The final ash weight was designated by W_{Ai} and the ash content (AC) of the samples was calculated using Eq. 3. The volatile matter content of the samples was determined according to ASTM E872 - 82 [26]. The weight loss due to devolatilization (corrected for moisture as determined in method E1756-08) is the volatile matter content and is calculated according to Eq. 3.

$$VM(\%) = \frac{w_i - w_f}{w_i} \times 100 \quad (2)$$

Where W_i is the corrected initial weight of the LBs, and

W_f is the final weight of the sample's residue after devolatilization. The fixed carbon (FC) content of the samples was determined after knowing the values of MC, AC, and VM according to Eq. 4.

$$FC = 100 - (MC + AC + VM) \quad (3)$$

Moreover, the elemental composition (carbon, hydrogen, nitrogen, and oxygen) was determined using an EA 1112 Flash NS/O elemental analyzer. Activation temperature range of the flax straw powder was determined by using thermogravimetric analyzer (TGA). The surface functional groups were analyzed using Fourier transform infrared (FTIR) spectroscopy (FTIR-is50ABx). The surface morphology of the FS-AC was observed using a scanning electron microscopy (SEM) Inspect F50 USA device. The crystal structure of the activated carbon was analyzed using an X-ray diffractometer (XRD-7000). The surface area, micropore volume, and micropore surface area of the activated carbons were determined using the Brunauer-Emmett-Teller (BET) (SA 9600) method.

2.4. Nitrate Adsorption Studies

Batch adsorption experiment was conducted with synthetic wastewater. 1.5236 g of KNO_3 was dissolved into 1.0 L distilled water to form nitrate stock solution with concentration of 1000 mg L^{-1} . The stock solution was diluted with distilled water in order to create nitrate solution with reduced concentration to produce synthetic wastewater solution. The experiments were carried out in 250 ml conical flasks by mixing a pre-weighted amount of adsorbent with 100 ml of nitrate solution. The nitrate adsorption onto FS-AC was carried out at room temperature ($30 \pm 1^\circ\text{C}$). The batch experiments were conducted to determine the efficiency of the adsorbent by controlling parameters (pH, adsorbent dosage, and contact time) on the removal of nitrate from the aqueous solution.

For this experiment, pH are 2, 7, and 9 were selected and dosages of 0.5, 1.0, and 1.5 g and contact time 60, 90, and 120 min were chosen with the use of $125 \text{ }\mu\text{m}$ particle-sized activated carbon. The pH was adjusted to different values using 0.1 M NaOH and 0.1 M HCl solution. The flasks were agitated in orbital shakers at 400 rpm.

Then, the agitated samples were filtered using Whatman (No.42) filter paper [27]. The initial and remaining nitrate ion concentrations were determined by using UV-vis spectrophotometer (UV-1800, Shimadzu). A wavelength of 450 nm was used for recording the UV-vis spectrum. Finally, percentage removal of nitrate ion (NO_3^-) was calculated with the help of Eq. 5.

$$\text{Percentage of nitrate removal} = \frac{C_i - C_f}{C_i} \times 100 \quad (4)$$

where, C_i and C_f are the initial and final nitrate levels in water (mg L^{-1}), respectively.

By knowing the nitrate concentrations before and after adsorption with FS-AC, the efficiency of nitrate ion adsorption can be determined. The adsorption efficiency of the nitrate at equilibrium (q_e) was determined using Eq. 6.

$$q_e = \left(\frac{C_i - C_e}{m} \right) v \quad (5)$$

where C_i and C_e are the initial and final concentration of nitrate ion (mg/L), v is the volume of solution (L), and m is the mass of adsorbent (g).

2.5. Statistical Analysis

For statistical data analysis and modeling of nitrate ion (NO_3^-) adsorption, Design Expert version 13.0 software (Stat-Ease, Minneapolis, USA), more especially, the response surface methodology (RSM) using CCD was utilized in this investigation. The statistical analysis included ANOVA analysis, model fitness testing, and model selection. P-value, R-squared value, and lack of fit were used in a model selection and fitness test. The interaction between the process factors and their impact on the result variable were ascertained using ANOVA analysis. The pH, contact time, and adsorbent dose were set as the independent variables while removal efficiency was the dependent variable for linear regression. A none transformed second-order polynomial regression was used to evaluate the magnitude and direction of each parameter [pH (A), initial concentration of nitrate ion (NO_3^-) (B), adsorbent dose (C), and contact time (D)], as well as their interaction with the response variable [AC removal efficiency]. Lastly, the 3D plots show how all the different things work together and give you a simple way to see how they change results. This big look shows how helpful statistical modeling is in environmental stuff, especially when we need to get rid of pollutants.

2.6. Adsorption Isotherms

Various adsorption isotherm models have been studied to understand the relationship between the amount of nitrate adsorbed and its concentration. The experimental procedure followed was based on the literature by Mahendran et al. [27]. Isotherms were determined using nitrate concentrations of 0.5, 1.0, 1.5, and 2.0 mg/L . The experimental conditions were set with a shaking speed of 400 rpm, pH of 2.0, adsorbent dosage of 1.5 g/L , solution temperature of 30°C , and contact time of 60 min.

2.7. Adsorption Kinetics

For kinetic studies, the following experimental conditions were maintained: 0.15 g of adsorbent, 100 mL of solution, initial nitrate concentration of 1 mg/L , shaking speed of 300 rpm, solution temperature of 30°C , and initial pH of 2. During this study, solutions were analyzed at 15, 30, 60, 90, and 120 min. Various kinetic models were tested to fit the experi-

mental data.

2.8. Adsorption Thermodynamics

Thermodynamic parameters provide useful information about internal energy changes during adsorption. Temperature studies were performed at 25, 35, 45, and 55 °C. An adsorbent dosage of 0.15 g was added to 100 mL of a 20 mg/L nitrate solution at pH 2.

3. Results and Discussion

3.1. Proximate and Ultimate Analysis

Table 1 displays proximate analysis of raw flax straw (FS) and its corresponding activated carbon (FS-AC) treated with H_3PO_4 at an impregnation ratio of 0.75 and carbonation time of 90 minutes.

Table 1. Proximate analyses (% wt.) of flax straw and its activated carbon.

	Moisture	Volatile	Ash	Fixed carbon
RFS (precursor)	4.6	71.01	6.04	18.35
FS-AC-400°C	8.41	57.21	9.88	24.5
FS-AC-500°C	7.62	52.02	17.87	22.49
FS-AC-600°C	6.41	48.11	18.82	26.66

As shown in Table 1, the proximate analysis of raw flax straw (RFS) is 4.6% which is comparable with other biomass-based activated carbon precursors, such as durian shell (5.853%) [28], castor hull (4.4%) [23] and almond shell (6.55%) [29] etc. The moisture contents of the prepared activated carbons prepared at 400 °C, 500 °C, and 600 °C are 8.41%, 7.62 and 6.41%. The increased moisture content of the activated carbon may be attributed to its affinity for water molecules compared to its procurer [23]. The values of volatile matters decrease from 71.01% (for raw flax straw) to 48.11% for FS-AC-600°C impregnated with H_3PO_4 with an impregnation ratio of 0.75- and 90-min carbonation time. As expected, the ash content and fixed carbon compositions increased with activation, while the volatile component's composition decreased.

The volatile component in the final activated carbon is greater than the value published for other biomass-based activated carbons, although the composition of the volatile components of the present precursor is equivalent to the values reported for other biomass precursors (Table 5). This might be due to the use of low impregnation ratio used in the current works. The ash content of the raw flax straw was

slightly higher than the values for the biomass depicted, and lower than the values reported for some biomasses such as tomato stems (10.6%) and tomato leaves (25.72%) [29]. Furthermore, it is evident that the current activated carbon has larger fixed carbon and ash concentrations at higher temperatures. Additionally, the fixed carbon for flax straw is comparable to the reported values for the majority of biomasses shown in Table 3. Nevertheless, compared to activated carbons made from other biomasses, the fixed carbon contents in FS-AC are substantially lower as shown in Table 4.

Table 2 shows the ultimate analysis of the RFS and the consequent FS-AC. As can be observed, RFS had a carbon content of 54.96%, whereas the activated carbon values for AC-400, AC-500, and AC-600 degrees Celsius are 63.22%, 64.66%, and 64.81%, respectively. Conversely, with AC-600 °C, the oxygen content dropped from 39.15% to 31.44%. The RFS has a carbon content of 46.64%, which is similar to the majority of the precursors listed in Table 3. A suitable antecedent for achieving high quality and the best yield of AC has more carbon in its biomass [23]. Comparable to other activated carbons made from other biomasses shown in Table 5, the activated carbon in this study has a comparable carbon content.

Table 2. Ultimate analysis of raw flax straw and its activated carbon.

	C	H	N	O
RFS (precursor)	54.96	5.68	0.21	39.15
FS-AC-400°C	63.22	3.26	0.52	33.0
FS-AC-500°C	64.66	3.01	0.78	31.55

	C	H	N	O
FS-AC-600°C	64.81	3.22	0.53	31.44

Table 3. Comparison of proximate and ultimate analysis of flax straw with different biomass.

Biomass	Proximate analysis (wt.%)				Ultimate analysis (wt.%)					References
	MC	Ash	VM	FC	C	H	N	O	S	
Castor hull	4.40	6.71	72.05	16.84	44.23	5.49	0.22	50.10	n.d	[23]
Paulownia wood	3.50	1.05	76.54	18.91	45.83	6.29	0.40	47.48	n.d	[30]
Fox nut	4.0	5.0	70.1	20.9	42.30	4.30	0.82	52.51	0.07	[15]
Acai seed	n.d	1.75	68.7	24.41	43.29	5.98	1.29	47.59	0.10	[31]
Durian shell	5.53	2.52	69.59	22.36	60.31	8.47	3.06	28.06	0.10	[28]
Euphorbia rigida	3.0	6.4	76.8	13.8	49.56	5.16	1.20	44.08	n.d	[32]
Eucalyptus wood	5.0	4.8	80.48	14.65	48.2	6.2	<0.5	44.1	<0.1	[33]
Flax straw	4.6	6.04	71.01	18.35	54.96	5.68	0.21	39.15	n.d	This study

n.d: not determined.

Table 4. Compression of proximate and ultimate analysis of flax straw activated carbon with activated carbon obtained from other biomass.

Biomass	Treatments		Proximate analysis (wt.%)				Ultimate analysis (wt.%)					References
	Chemical	Thermal	MC	Ash	VM	FC	C	H	N	O	S	
Castor hull	H ₃ PO ₄	800°C	6.32	19.10	49.56	27.76	63.88	3.13	0.52	32.47	n.d	[23]
Paulownia wood		400°C	2.30	2.63	17.80	77.27	70.83	3.41	n.d	25.76	n.d	[30]
Fox nut	H ₃ PO ₄	700°C	3.12	2.12	21.05	73.71	64.85	4.52	1.24	29.24	1.15	[15]
Soyabeans pod	H ₃ PO ₄	305.34 °C	4.67	6.90	34.78	53.65	71.48	15.55	n.d	9.27	3.7	[34]
Flax straw	H ₃ PO ₄	600 °C	5.53	12.22	47.36	34.89	66.26	3.18	0.11	30.45	n.d	This study

n.d: not determined.

3.2. Thermogravimetric Analysis

The thermogravimetric analysis (TGA) experiment was conducted with an initial mass of 10 mg at a ramping rate of 10 K/min from 25 to 800 °C. Figure 2 illustrates the TG-DTG-DTA analysis of the raw flax straw. The moisture and highly volatile compounds are removed up to a temperature of about 220°C. In this stage, about 5.1% of the initial pressure was lost. Sharp weight losses were observed when the temperature rises from 220 to 380°C which eliminates

volatile matters and tars due to carbonization or active pyrolysis [23]. In the second stage, about 44.13% of the total initial weight was removed. The third stage (380-510°C) with a weight loss of 18.91% corresponds to the decomposition of structurally stable components of the biomass. Beyond 510°C, less weight loss was observed due to the decomposition of lignin of which decomposition may take place at higher temperatures and the weight loss becomes approximately constant from 560°C. The total weight loss at around 560°C is about 74.1% which shows calcination without H₃PO₄ impregnation provides a low AC yield.

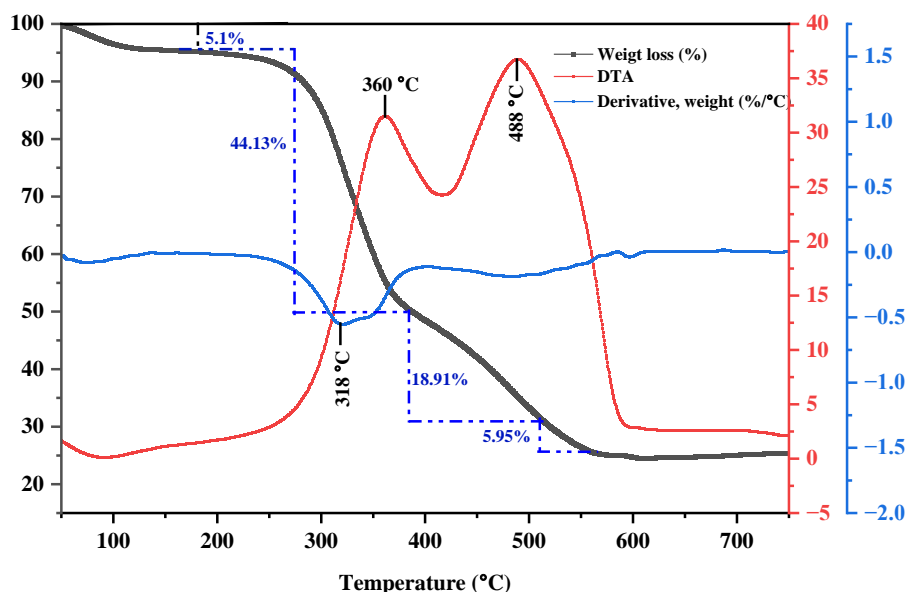


Figure 2. TG-DTG-DTA curve for raw flax straw.

Essentially, as shown in the Figure 2, DTG measures the rate of material degradation; sharp peaks around 318 °C show that the flax straw is breaking down quickly, and DTA pinpoints the thermal events (energy shifts) that propel those processes. Exothermic processes (heat release) are shown by negative peaks, whereas endothermic reactions (heat absorption) are indicated by positive peaks.

3.3. SEM Analyses

Figure 3 displays the SEM image of the FSAC. The natural fibrous structure of flax straw is depicted in Figure 3(a),

where the unprocessed state is reflected by the elongated, ribbon-like strands that provide a comparatively smooth surface. The activated carbon, on the other hand, is depicted in Figure 3(b) after undergoing a transition that has produced an irregular, extremely porous structure with a significant number of tiny pores. These pores, which differ in size and form, greatly increase the porosity and surface area of the material. This morphological alteration highlights the potential of turning biomass into useful, high-performance materials for environmental remediation by optimizing the activated carbon for adsorption applications, namely in the removal of nitrate ions from aqueous solutions.

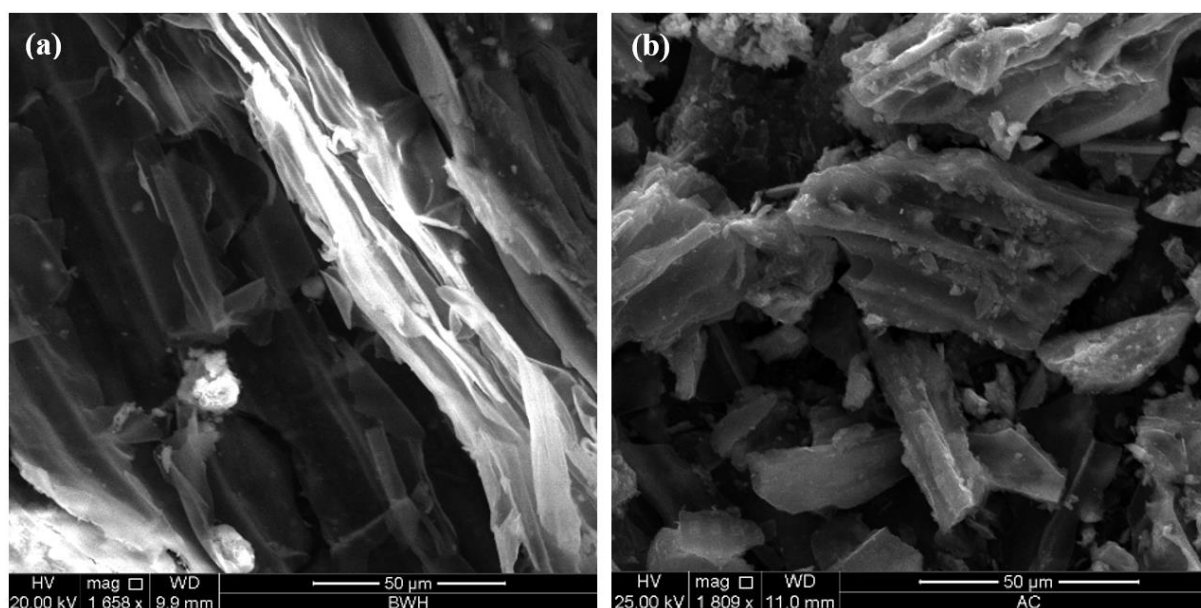


Figure 3. SEM images. (a) Raw flax straw and (b) the prepared activated carbon.

3.4. FTIR (Fourier Transform Infrared Spectroscopy) Analysis

Fourier Transform Infrared (FTIR) spectra of raw flax straw (FS) and its activated carbon (FS-AC) are shown in Figure 4. The raw flax straw spectrum (blue) shows a number of significant absorption peaks. Interestingly, the stretching vibration of hydroxyl (-OH) groups is represented by a large peak at about 3320 cm^{-1} , which suggests the presence of moisture and different alcohols [23]. The peak around 2920 cm^{-1} , which represents the amount of lignin and cellulose, is ascribed to the C-H stretching vibrations of alkyl groups. Furthermore, the peak at about 1730 cm^{-1} shows carbonyl groups' C=O stretching vibrations, which are typical in hemicellulose [14].

On the other hand, there are notable alterations in the spectrum of the activated carbon, which is displayed in black. The reduction of the wide -OH signal at 3320 cm^{-1} indicates that some hydroxyl functional groups were eliminated during activation. The C=O peak around 1730 cm^{-1} is diminished or absent, indicating that carbonyl groups have been largely eliminated [23], which can enhance the adsorption capabilities of the activated carbon. The formation of a more graphitic structure is indicated by the peak that may appear at about 1620 cm^{-1} , which represents C=C stretching [35].

The chemical changes that take place when raw flax straw is transformed into activated carbon are reflected in these spectral shifts, which improve the material's surface qualities and qualify it for uses such as the extraction of nitrate ions from aqueous solutions. The FTIR analysis shows how well the activation process works to improve the material's adsorptive properties by offering insightful information about the changes in the functional groups [35, 36].

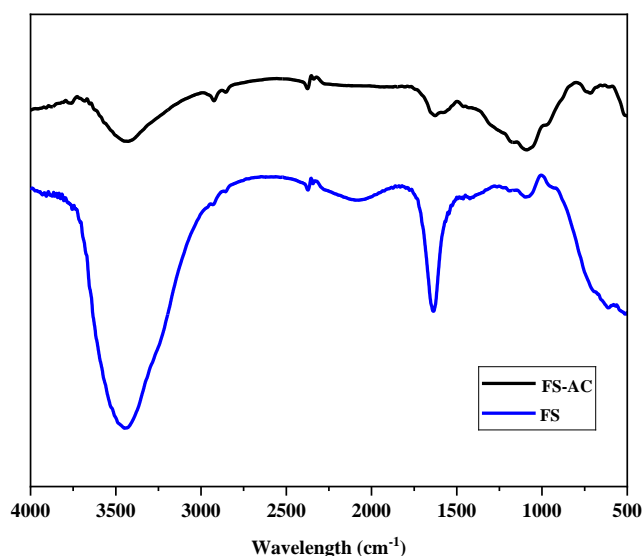


Figure 4. FTIR spectrum of flax straw and its activated carbon.

3.5. XRD Analysis of FS-AC

Figure 5 displayed the synthesized TSACs of the XRD spectrum. A low degree of crystallinity or a small crystallite size in the carbon structure is indicated by the large diffraction background, which is equivalent to a 2θ angle between 30° and 40° in the spectrum. Activated carbons are known for their irregular structure, and this is one of its characteristics. The existence of crystalline impurities is suggested by the XRD peaks found in the FS-activated carbon (activated carbon generated from flax straw) at 29.6° , 36.2° , 43° , 56° , and 63° . By improving the material's adsorptive properties, this structural configuration makes it appropriate for uses including eliminating impurities, such as nitrate ions, from aqueous solutions.

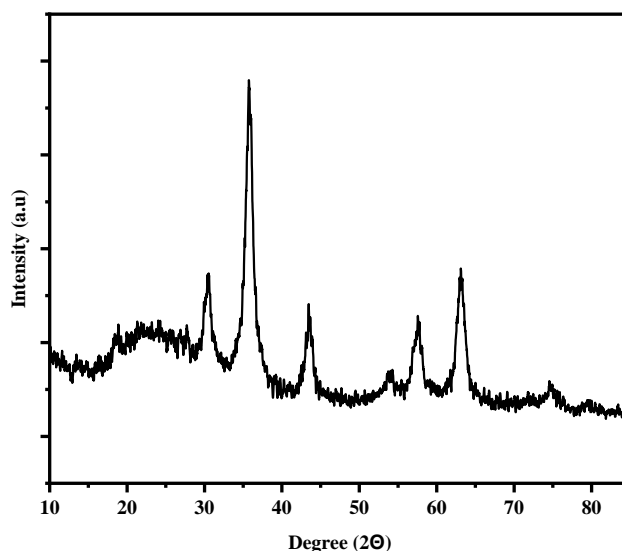


Figure 5. X-ray diffraction of FS-activated carbon.

3.6. Brunauer-Emmett-Teller (BET) Analysis

The Brunauer-Emmett-Teller (BET) method, a well-known approach for describing porous materials, was used to calculate the surface area of the produced flax straw activated carbon (FS-AC). This technique is very helpful for figuring out surface area, pore size, and pore volume since it measures the physical adsorption of gas molecules on a solid's surface [14]. According to this investigation, the activated carbon from flax straw has a BET surface area of $798.23\text{ m}^2/\text{g}$. An important component of activated carbon's effectiveness as an adsorbent is its high surface area, which suggests a sizable quantity of surface area available for adsorption.

3.7. Adsorption Studies

Adsorption studies were performed on FS-AC prepared at the optimum activation parameters. The effect of adsorbent

dosage, time, pH, and initial nitrate ion concentration was studied.

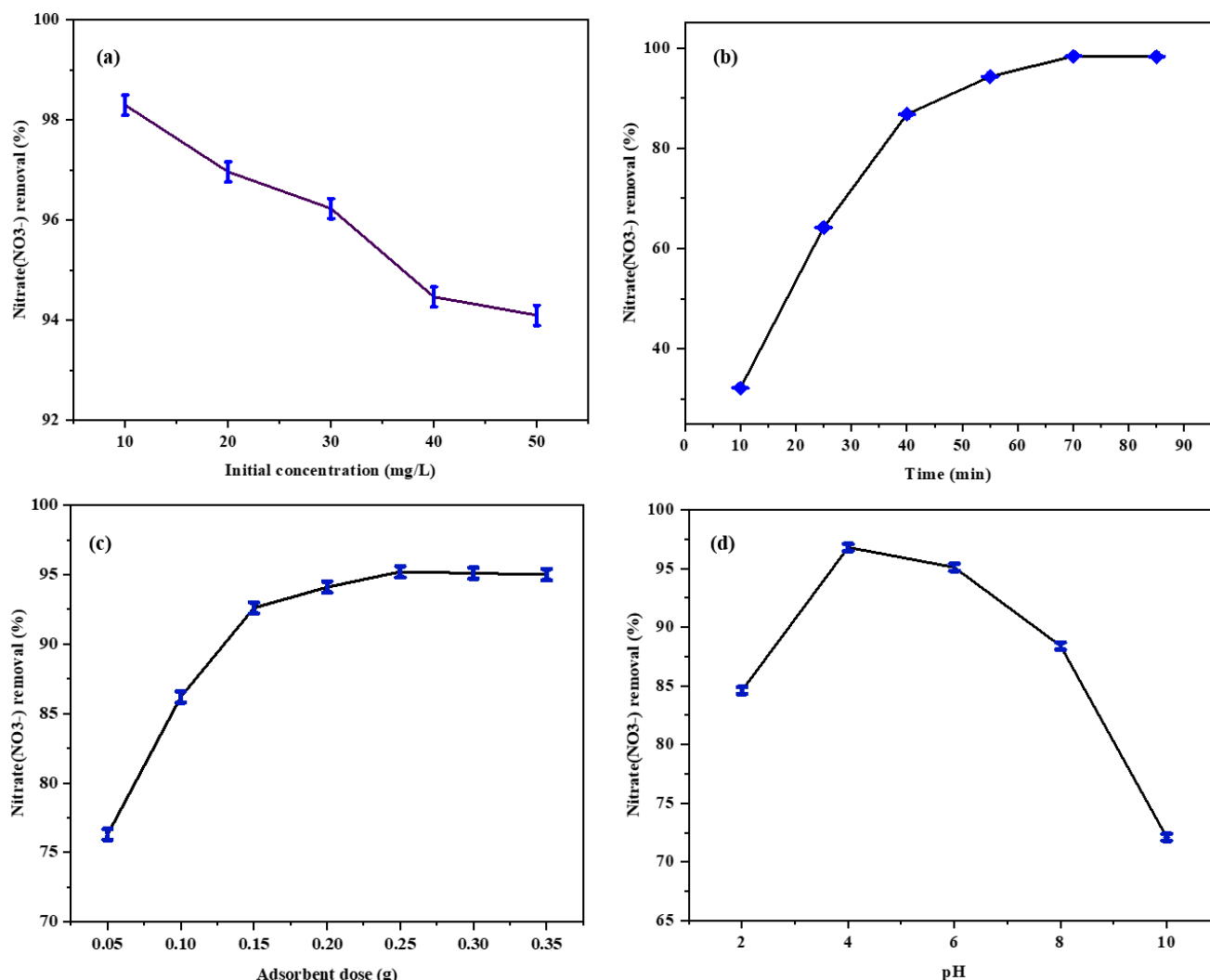


Figure 6. Adsorption parameters impact on the percentage of nitrate (NO_3^-) ion removal. (a) initial concentration of nitrate (NO_3^-) ion, adsorption time, adsorbent dosage and (d) pH.

3.7.1. Effect of Contact Time on Adsorption

Figure 6(b) illustrates the findings of adsorption investigations as a function of adsorption time. The percentage of nitrate ions eliminated increases from 35% to 89% when the contact time is extended from 10 to 40 minutes. The availability of additional active sites during the initial stages of adsorption may be the cause of this increase [37]. After 60 minutes, the elimination percentage did not, however, increase noticeably. The adsorbents are kept from filling the empty gaps by a growing repulsive force between the adsorbate ions with time, which is the main reason why the adsorption efficiency does not rise much. An adsorption time of 60 minutes produced a maximum removal effectiveness of 98.4%. Since there are no more free active sites and adsorption occurs at equilibrium circumstances, the nitrate ion removal percentage does not increase after the optimal period of

time [14]. In general, the adsorption process started off quickly and slowed down as the number of potential adsorption sites decreased [14, 27, 37].

3.7.2. Effect of Adsorbent Dose on Adsorption

A key factor in achieving the best adsorption outcomes while reducing adsorbent loss is determining the appropriate amount of adsorbent. The elimination efficiency of FS-AC rises from 76% to 95.2% when the dose of activated carbon is raised from 0.05 g/L to 0.25 g/L, as shown in Figure 6(c). This might be because there are more adsorption sites accessible for the metal ion [14]. However, the removal effectiveness drops to 95% as the adsorbent dose increases from 0.25 g/L to 0.35 g/L. This might be because high adsorbate concentrations cause adsorbents to aggregate and obstruct the AC's active sites, which lowers the adsorbent's active surface area [37]. Thus, peak nitrate ion removal was achieved with an

adsorbent dosage of 0.25 g/L of the solution.

3.7.3. Effect of Initial Concentration of Nitrate Ion on Adsorption

The relationship between the initial concentration of nitrate (NO_3^-) and its removal efficiency is shown in Figure 6(a). The removal efficiency shows a declining trend as the starting nitrate concentration rises from 10 mg/L to 50 mg/L. In particular, the removal efficiency steadily decreases to around 94% at higher doses after beginning at about 98% for lower values. This is due to the reason that higher initial nitrate concentrations may hinder the effectiveness of the removal process, leading to a less efficient reduction in nitrate levels in the solution [37]. Therefore, for low nitrate ion concentrations, we can say that the starting concentration has a higher influence. This is due to a higher ratio of adsorption sites to total ions in the solution at lower nitrate (NO_3^-) concentrations. By interacting with the adsorbent, all of the nitrate (NO_3^-) ions can finally be eliminated from the solution [36, 37].

3.7.4. Effect of Solution pH on Adsorption

The effect of pH on nitrate (NO_3^-) removal efficiency is depicted in Figure 6(d). The removal efficiency improves with pH from 2 to 6, reaching a peak of about 96% at pH 4. After this, though, the removal efficiency starts to decrease as

the pH rises further near 10. The initial increase shows that a more acidic to neutral environment enhances the nitrate removal process, while the subsequent decrease at higher pH levels indicates that excessively alkaline conditions may negatively impact the removal efficiency. At pH 4, nitrate (NO_3^-) was better removed, whereas under extremely acidic and moderately basic conditions, removal was reduced. Tessema et al. [36] and Yirdaw et al. [37] obtained a similar result. The total surface charge on the active site rises to a positive at a very acidic pH, and protons and metal cations vie for the adsorbent's binding site [37]. Similar patterns have been documented for Pb (II) ion adsorption on activated carbon made from various biomasses [36, 37].

3.8. Response Surface Methodology

Using response surface methods based on central composite design (CCD), the effects of three FSAC treatment parameters (activation temperature, impregnation ratio, and H_3PO_4 concentration) on the removal of nitrate ions from the resulting activated carbon were investigated. Table 5 displays the design matrix of parameters as well as the proportion of projected and experimental nitrate ion removal. In this particular case, A, B, and C stand for the H_3PO_4 concentration, impregnation ratio, and activation temperature, respectively.

Table 5. Activated carbon prepared from flax straw and its corresponding response to the CCD design matrix.

Run	Activated carbon preparation parameters			Response		Residual
				Nitrate removal percentage (%)		
	A	B	C	Experimental	Predicted	
1	2	5	500	91.53	91.46	0.07
2	2	5	631.60	88.5	88.45	0.052
3	2	6.32	500	89.8	89.79	0.014
4	2	3.68	500	87.5	87.55	-0.045
5	3	6	600	90.31	90.23	0.076
6	2	5	500	91.57	91.46	0.11
7	2	5	500	91.57	91.46	0.11
8	1	4	400	88.78	88.84	-0.063
9	3.32	5	500	92.5	92.55	-0.048
10	2	5	500	91.07	91.46	-0.39
11	3	4	400	88.5	88.36	0.141
12	2	5	500	91.53	91.46	0.07
13	2	5	500	91.53	91.46	0.07
14	1	4	600	89.8	89.73	0.075

Run	Activated carbon preparation parameters			Response		Residual
				Nitrate removal percentage (%)		
	A	B	C	Experimental	Predicted	
15	2	5	368.39	88	88.08	-0.083
16	0.68	5	500	93.34	93.32	0.016
17	1	6	400	87.2	87.1	0.099
18	3	6	400	90.5	90.56	-0.061
19	3	4	600	85	85.09	-0.086
20	1	6	600	90.8	90.93	-0.127

Table 5 displays predicted and experimental nitrate removal efficiency (%) as well as residual values for 20 activated carbon preparation runs with three important parameters changed: A (activation temperature, °C), B (impregnation ratio), and C (H_3PO_4 concentration, mol). The nitrate removal efficiencies in the experimental findings range from 85.00% (Run 19) to 93.34% (Run 16). The residuals, or the difference between the experimental and predicted values, are generally minimal ($\leq \pm 0.39\%$), showing strong model accuracy. High

concentration and temperature have a negative synergy. Run 16 had the best performance (0.68 mol H_3PO_4 , 500 °C), whereas Run 19 had the lowest efficiency (3 mol H_3PO_4 , 600 °C). Stable efficiency ($\sim 91.5\%$) were obtained under central settings (Runs 1, 6, 12), confirming the resilience of mid-range parameters. The information emphasizes how important it is to strike a balance between preparatory variables and how they all affect adsorption effectiveness.

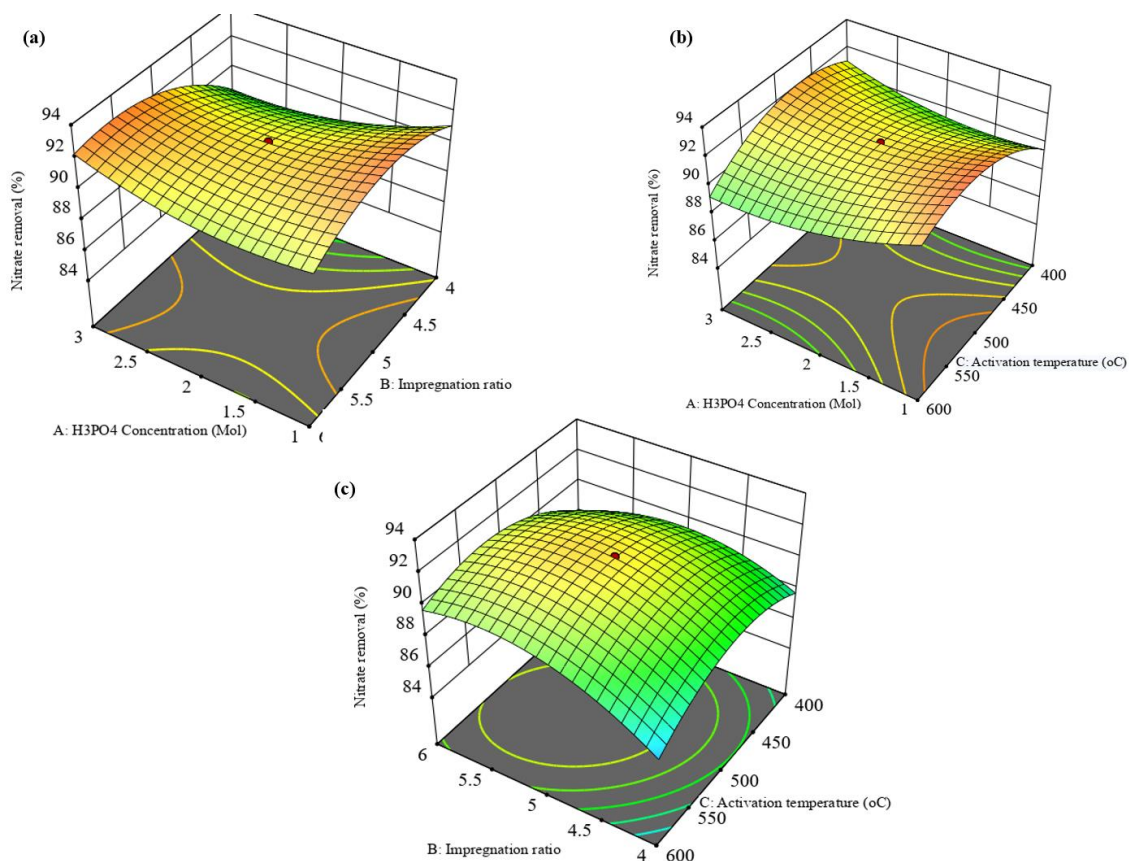


Figure 7. Response surface plots illustrating the effects of activation temperature, impregnation ratio, and H_3PO_4 concentration on nitrate removal efficiency.

Through response surface plots, Figure 7 shows how the concentration of H_3PO_4 (A), the impregnation ratio (B), and the activation temperature (C) interact to affect the efficiency of nitrate removal. The graphs show that synergistic conditions increase nitrate removal: moderate activation temperatures (500-600 °C) combined with lower H_3PO_4 concentrations (0.68-2 mol) improve adsorption effectiveness, probably as a result of ideal pore formation and surface activation. Efficiency is decreased at higher temperatures (>600 °C) and H_3PO_4 concentrations (>3 mol), which may indicate chemical over-saturation or thermal deterioration of the adsorbent.

The impregnation ratio (5-6) also exhibits a parabolic connection; departures from this range, either too high (>6) or too low (<5), upset the equilibrium between pore accessibility and surface modification. Notably, efficiency losses are made worse by the combination of high impregnation ratios and high temperatures, whereas maximal performance (~93.6%) is obtained with low H_3PO_4 concentrations and moderate temperatures.

3.9. Adsorption Isotherms

The relationship between the concentration of the nitrate solution and the quantity that the adsorbent's surface will adsorb is indicated by the adsorption isotherm [27]. In order to fully understand the adsorption mechanism and the maximum adsorption capacity of the FSAC, the experimental data in this work were fitted using the Langmuir and Freundlich isotherm models. To determine which isotherm model best fits the adsorption experiment, the findings of a study into the adsorption behavior of nitrate ions employing FSAC adsorbent were compared using the coefficient of correlation, or R^2 . Under optimal conditions (pH = 4, adsorbent time = 70 min, FSAC dose = 0.25 g/100 mL, and agitation speed = 200 rpm), the initial lead ion concentration was varied between 10 and 50 mg L^{-1} during the adsorption isotherm experiment, which was conducted at room temperature (25 °C). To determine if these models were reliable, the models utilized to examine the equilibrium adsorption data are shown in Figure 7.

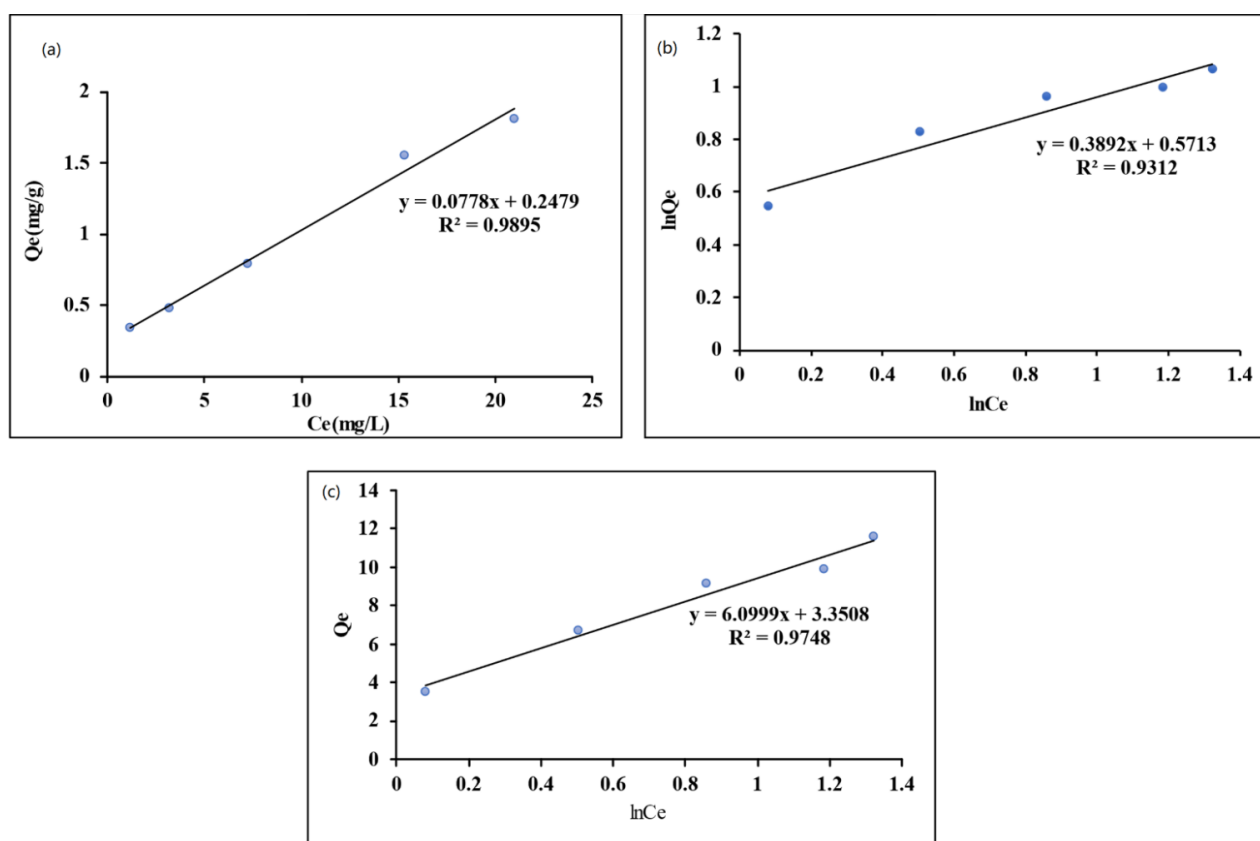


Figure 8. Plot of isotherm models (a) Langmuir, (b) Freundlich, and (c) Temkin isotherm models.

Table 6. Isotherm constants for the adsorption of nitrate on flax straw activated carbon.

No	Isotherm models	Equation	Parameters	R^2 value
1	Langmuir isotherm	$Q_e = \frac{q_m + K_L C_e}{1 + K_L C_e}$	$q_m = 1.286 \text{ mg/g}$, $K_L = 0.313 \text{ L/mg}$	0.9895

No	Isotherm models	Equation	Parameters	R ² value
2	Freundlich isotherm	$Q_e = K_f C_e^{\frac{1}{n}}$	$K_f = 1.77 \text{ mg/g}, n = 2.57$	0.9312
3	Tempkin isotherm	$Q_e = \frac{RT}{b} \ln(K_T C_e)$	$KT = 1.73 \text{ L/g}, b = 406.2 \text{ J/mol}$	0.9748

Based on the R² values and the closeness of the model predictions to the experimental data provided in Table 5, the Langmuir isotherm (R²=0.9895) is the best-fitting model for the adsorption of nitrate onto flax straw activated carbon. Table 6 shows the comparison among the best-known isotherm models.

Table 7. Isotherm model fit summary.

Isotherm model	R ² value	Interpretation
Langmuir	0.9895	Best fit, closest to 1.0. indicates monolayer adsorption on homogeneous surfaces.
Temkin	0.9748	Good fit, indicates uniform binding energy distribution.
Freundlich	0.9312	Least fit, implies heterogeneous surface adsorption.

3.10. Adsorption Kinetic Study

Utilizing a 100 mL solution with initial concentration = 70 mg L⁻¹, PH = 4, adsorbent dose = 0.25 g/100 mL, and agitation speed = 200 rpm) at room temperature, the FSAC adsorbent was used in the adsorption kinetics studies, which varied the contact time for lead removal from 10 to 85 min while keeping other parameters at their ideal values. To ascertain which model best suited the adsorption experiment, the data were compared. The kinetic data were fitted to pseudo-first-order (PFO) and pseudo-second order (PSO)

models, as shown in Figure 7. The constants for these kinetic models are listed in Table 7.

The adsorption kinetics data were fitted to Pseudo-First-Order (PFO) and Pseudo-Second-Order (PSO) models, yielding comparable R² values of 0.9395 and 0.9408, respectively as shown in Table 7. Despite the strong correlation between the two models, the PSO model's slightly higher R² indicates that it more accurately captures the adsorption mechanism, which is most likely chemisorption. The difference between the experimental Q_e (23.5 mg/g) and the projected Q_e values (47.6 vs. 41.0 mg/g), however, emphasizes the necessity of verifying hypotheses against actual data.

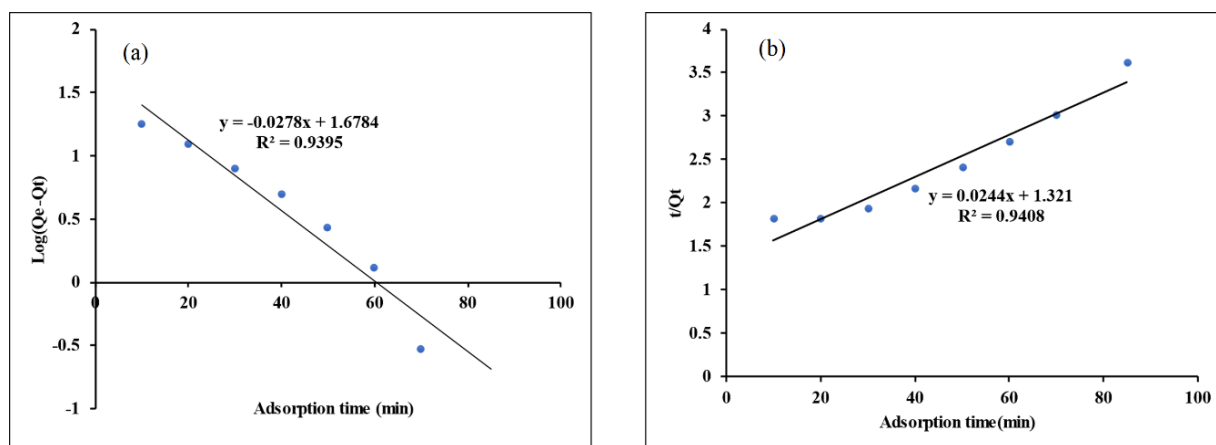


Figure 9. Fit curves of two kinetic models for adsorption of nitrate by FSAC (a): pseudo-first order; (b): pseudo-second-order.

Table 8. Kinetic parameters for adsorption of nitrate on flax straw activated carbon.

Model	Equation	Constants	Q _e (mg/g)	R ²
Pseudo-First-Order	$\log(Q_e - Q_t) = \log Q_e - \frac{K_1}{2.303} xt$	$K_1 = 0.064 \text{ min}^{-1}$	47.6	0.9395
Pseudo-Second-Order	$\frac{t}{Q_t} = \frac{1}{K_2 Q_e^2} + \frac{1}{Q_e} xt$	$K_2 = 0.00045 \text{ g/mg.min.}$	41.0	0.9408

3.11. Adsorption thermodynamics

The Van't Hoff equation was used to compute thermodynamic parameters, such as the free energy change (ΔG°), enthalpy change (ΔH°), and entropy change (ΔS°). The thermodynamic adsorption parameters (ΔH°), (ΔS°) and (ΔG°), enthalpy change (ΔH°), and entropy change (ΔS°) have been obtained by Eq.6 as described previously by Nassar et al. [35].

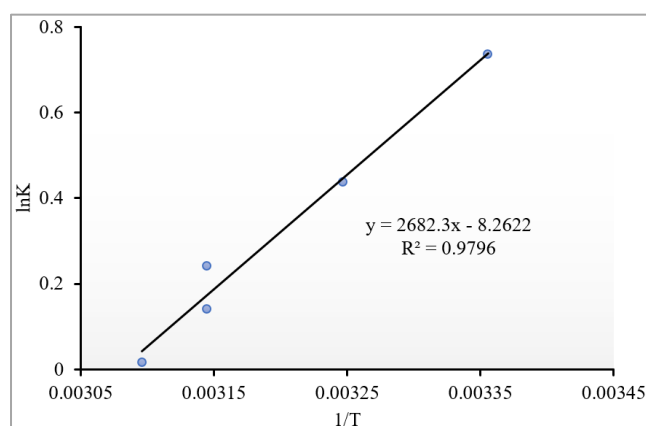
$$\ln K = \frac{\Delta S^\circ}{(R)} - \frac{\Delta H^\circ}{(RT)} \quad (6)$$

where T (K) is the absolute solution temperature (298 K), K_d is the distribution coefficient that may be computed using Eq.7, and R (8.314 J/mol K) is the gas constant.

$$K = C_{Ae} / C_e \quad (7)$$

where C_{Ae} (mg/L) is equilibrium amount adsorbed on solid surface, C_e (mg/L) is the equilibrium solution concentration.

Slopes and intercepts of plots of lnK vs. (1/T), shown in Figure 8, are used to determine values of ΔH° and ΔS° . Table 8 provides a summary of thermodynamic parameters. Eq. 6 was used to get the distribution coefficient (K).

**Figure 10.** Adsorption data is fitted to the lnK vs. (1/T) plot.**Table 9.** Values of adsorption thermodynamic parameters at different temperatures.

Adsorbent	ΔH° (kJ/mol)	ΔS° (J/mol K)	ΔG (kJ/mol)				
			298 K	308K	313 K	318 K	323 K
FSAC	-14.19	-43.38	-1.27	-0.84	-0.62	-0.40	-0.18

All ΔG° values are negative, as shown in Table 8, indicating that the adsorption process is spontaneous at all investigated temperatures. An exothermic process (where heat is released) is indicated by a negative ΔH° . Adsorbate molecules lose their freedom when they bond, as indicated by the negative ΔS° . These findings are consistent with physisorption-dominated adsorption processes (e.g., van der Waals forces).

4. Conclusions

The conversion of flax straw (*Linum usitatissimum* L.) into

high-performance activated carbon (FS-AC) through phosphoric acid (H_3PO_4) activation for nitrate removal from aqueous solutions was successfully proven in the study. A highly porous structure with a surface area of 798.23 m²/g was observed upon characterization using SEM and BET analysis, demonstrating greater adsorption capacity as a result of more active sites. Nitrate adsorption was facilitated by electrostatic interactions and surface complexation in an amorphous carbon matrix with residual crystalline phases, as revealed by XRD and FTIR studies. Moderate activation temperatures (500-600 °C), lower H_3PO_4 concentrations (0.68-2 M), and balanced impregnation ratios (5-6) were shown to be the ideal preparation conditions through

optimization using response surface methodology (RSM). With these parameters, FS-AC removed 98.4% of the nitrate at pH 4, 0.25 g/L dosage, and 60 minutes of contact time. The study addresses the issues of waste valorization and water pollution by highlighting the dual environmental advantages of turning agricultural flax straw waste into a sustainable adsorbent. With a high fixed carbon content (up to 34.89%) and effective nitrate removal, FS-AC performed competitively when compared to activated carbons made from other biomasses. The combination of thorough characterization and statistical optimization (RSM) shed light on how adsorption mechanisms and preparation factors interact. Future research should concentrate on testing the effectiveness of FS-AC in actual wastewater matrices with co-existing contaminants, investigating regeneration cycles to increase cost-effectiveness, and scaling up production for industrial applications.

Abbreviations

FS-AC	Flax Straw Activated Carbon
SEM	Scanning Electron Microscopy
XRD	X-ray Diffraction
FTIR	Fourier Transform Infrared Spectroscopy
BET	Brunauer-Emmett-Teller
TGA	Thermogravimetric Analysis
DTG	Derivative Thermogravimetry
DTA	Differential Thermal Analysis
ANOVA	Analysis of Variance
PFO	Pseudo-First-Order
PSO	Pseudo-Second-Order
ASTM	American Society for Testing and Materials
MC	Moisture Content
VM	Volatile Matter
AC	Ash Content
FC	Fixed Carbon
EA	Elemental Analyzer
UV-vis	Ultraviolet-Visible
RFS	Raw Flax Straw
FS	Flax Straw
AG°	Gibbs Free Energy Change
AH°	Enthalpy Change
AS°	Entropy Change

Acknowledgments

Thanks to Debre Berhan university for accomplishing this work.

Author Contributions

Damenech Tefera Werku: Writing - original draft, Methodology, Investigation, Conceptualization

Getahun Yifru Desta: Writing - original draft, Supervision, Methodology, Investigation, Formal analysis, Concep-

tualization

Tayto Mindahun: Writing - review & editing, Writing - original draft, Visualization, Methodology, Investigation

Funding

There is no fund for this study.

Data Availability Statement

The data that has been used is confidential.

Conflicts of Interest

The authors declare no conflicts of interest.

References

- [1] R. Picetti et al., "Nitrate and nitrite contamination in drinking water and cancer risk: A systematic review with meta-analysis," *Environ. Res.*, vol. 210, 2022, <https://doi.org/10.1016/j.envres.2022.112988>
- [2] S. Dey, N. Haripavan, S. R. Basha, and G. V Babu, "Current Research in Chemical Biology Removal of ammonia and nitrates from contaminated water by using solid waste bio-adsorbents," *Curr. Res. Chem. Biol.*, vol. 1, 2021, <https://doi.org/10.1016/j.crchbi.2021.100005>
- [3] WHO, Guidelines for Drinking-water Quality. 2017.
- [4] W. S. Al-rashed and A. Lakhout, "Nitrate removal from drinking water using different reactor / membrane types: A comprehensive review," *Int. Res. J. Public Environ. Heal.*, vol. 9, no. 3, pp. 1-9, 2022.
- [5] F. Rezvani, M. Sarrafzadeh, and S. Ebrahimi, "Nitrate removal from drinking water with a focus on biological methods: a review," *Env. Sci Pollut Res BER*, 2017, <https://doi.org/10.1007/s11356-017-9185-0>
- [6] M. Khatamian, S. K. Derakhshan, S. H. Nami, and S. F. Shokouhi, "Nitrate removal study of synthesized nano γ - alumina and magnetite - alumina nanocomposite adsorbents prepared by various methods and precursors," *Sci. Rep.*, pp. 1-13, 2024, <https://doi.org/10.1038/s41598-024-58459-z>
- [7] R. Kumar, B. Singh, and B. Acharya, "A comprehensive review on activated carbon from pyrolysis of lignocellulosic biomass: An application for energy and the environment," *Carbon Resour. Convers.*, vol. 7, no. 4, 2024, <https://doi.org/10.1016/j.crcon.2024.100228>
- [8] N. Muttill, S. Jagadeesan, A. Chanda, and M. Duke, "Production, Types, and Applications of Activated Carbon Derived from Waste Tyres: An Overview," *Appl. Sci.*, 2023.
- [9] T. T. Hailemariam and B. Woldeyes, "Production and characterization of pulp and paper from flax straw," *Scientific reports*, pp. 1-16, 2024.

- [10] B. Vafakish, A. Babaei-ghazvini, M. Ebadian, and B. Acharya, "Pyrolysis and Combustion Behavior of Flax Straw as Biomass : Evaluation of Kinetic, Thermodynamic Parameters, and," *Energies*, 2023.
- [11] P. Cerny, M. Babenko, P. Bartos, Y. Kononets, P. Kriz, and R. Rabenseifer, "Complex Study of the Composite Building Material Based on Flax Straw Organic Waste : Hygrothermal and Physicochemical Properties," *Waste and Biomass Valorization*, vol. 15, no. 4, pp. 2231-2247, 2024, <https://doi.org/10.1007/s12649-023-02273-7>
- [12] M. S. Masoud, W. M. El-saraf, A. M. Abdel, A. E. Ali, E. A. Mohamed, and H. M. I. Hasan, "Rice husk and activated carbon for waste water treatment of El-Mex Bay, Alexandria Coast, Egypt," *Arab. J. Chem.*, vol. 9, pp. S1590-S1596, 2016, <https://doi.org/10.1016/j.arabjc.2012.04.028>
- [13] S. Mustefa, S. V. Prabhu, T. T. Sissay, and A. A. Getahun, "Sugarcane bagasse based activated carbon preparation and its adsorption efficacy on removal of BOD and COD from textile effluents : RSM based modeling, optimization and kinetic aspects," *Bioresour. Technol. Reports*, vol. 14, 2021, <https://doi.org/10.1016/j.biteb.2021.100664>
- [14] S. Shewatatek, G. Gonfa, and S. Mekuria, "Response Surface Optimization of Lead Adsorption onto Teff Straw-Derived Activated Carbon Response surface optimization of lead adsorption onto teff straw-derived activated carbon," *Results in Surfaces and Interfaces*, 2024, <https://doi.org/10.1016/j.rsufri.2024.100378>
- [15] A. Kumar and H. M. Jena, "Preparation and characterization of high surface area activated carbon from Fox nut (*Euryale ferox*) shell by chemical activation with H₃PO₄," *Results Phys.*, vol. 6, pp. 651-658, 2016, <https://doi.org/10.1016/j.rinp.2016.09.012>
- [16] R. Zakaria, N. A. Jamalluddin, M. Zailani, and A. Bakar, "Results in Materials Effect of impregnation ratio and activation temperature on the yield and adsorption performance of mangrove based activated carbon for methylene blue removal," *Results Mater.*, vol. 10, 2021, <https://doi.org/10.1016/j.rinma.2021.100183>
- [17] M. M. Alam et al., "The potentiality of rice husk-derived activated carbon: From synthesis to application," *Processes*, vol. 8, no. 2, 2020, <https://doi.org/10.3390/pr8020203>
- [18] E. H. Sujiono et al., "Fabrication and characterization of coconut shell activated carbon using variation chemical activation for wastewater treatment application," *Results Chem.*, vol. 4, 2022, <https://doi.org/10.1016/j.rechem.2022.100291>
- [19] Z. Liu et al., "Preparation, characterization and application of activated carbon from corn cob by KOH activation for removal of Hg (II) from aqueous solution," *Bioresour. Technol.*, vol. 306, 2020, <https://doi.org/10.1016/j.biortech.2020.123154>
- [20] E. Chavez, L. Alva, J. C. Altamirano-oporto, Y. Antonio, and S. Diaz, "Case Studies in Chemical and Environmental Engineering Evaluation of the efficiency of activated carbon filters based on coconut endocarp and rice husk for wastewater treatment," *Case Stud. Chem. Environ. Eng.*, vol. 11, 2025, <https://doi.org/10.1016/j.cscee.2025.101160>
- [21] R. Yimin, R. Abba, G. Dawut, A. Abdulkayum, and B. Xiong, "Preparation and Adsorption Performance of Walnut Waste-Based Magnetic Activated Carbon with High Specific Surface Area," *ACS Omega*, 2025, <https://doi.org/10.1021/acsomega.4c05032>
- [22] I. Neme, G. Gonfa, and C. Masi, "Activated carbon from biomass precursors using phosphoric acid : A review," *Heliyon*, vol. 8, p. e11940, 2022, <https://doi.org/10.1016/j.heliyon.2022.e11940>
- [23] I. Neme, G. Gonfa, and C. Masi, "Preparation and characterization of activated carbon from castor seed hull by chemical activation with H₃PO₄," *Results Mater.*, vol. 15, 2022, <https://doi.org/10.1016/j.rinma.2022.100304>
- [24] ASTM, "Standard Test Method for Determination of Total Solids in Biomass," 2015. <https://doi.org/0.1520/E1756-08.10.1520/E1756-08R15.2>
- [25] ASTM, "Standard Test Method for Ash in Biomass," 2020. <https://doi.org/1.1520/E1755-01R20.2>
- [26] ASTM, "Standard Test Method for Volatile Matter in the Analysis of Particulate Wood Fuels," 2019. <https://doi.org/1.1520/E0872-82R19.2>
- [27] M. Mahendran, S. Prabagar, S. Thuraisingam, and J. Prabagar, "Removal of nitrate ion from aqueous solution using palmyrah nut shell activated carbon : factorial optimization and equilibrium studies," *Discov. Civ. Eng.*, 2024, <https://doi.org/10.1007/s44290-024-00054-2>
- [28] T. Christine, M. Maria, J. Sunarso, Y. Sudaryanto, and S. Ismadji, "Activated carbon from durian shell : Preparation and characterization," *J. Taiwan Inst. Chem. Eng.*, vol. 40, pp. 457-462, 2009, <https://doi.org/10.1016/j.jtice.2008.10.002>
- [29] B. Tiryaki, E. Yagmur, A. Banford, and Z. Aktas, "Comparison of activated carbon produced from natural biomass and equivalent chemical compositions," *J. Anal. Appl. Pyrolysis*, vol. 105, pp. 276-283, 2014, <https://doi.org/10.1016/j.jaap.2013.11.014>
- [30] S. Yorgun and D. Yildiz, "Preparation and characterization of activated carbons from Paulownia wood by chemical activation with H₃PO₄," *J. Taiwan Inst. Chem. Eng.*, vol. 53, pp. 122-131, 2015, <https://doi.org/10.1016/j.jtice.2015.02.032>
- [31] L. S. Queiroz et al., "Activated carbon obtained from amazonian biomass tailings (acai seed): Modification, characterization, and use for removal of metal ions from water," *J. Environ. Manage.*, vol. 270, 2020, <https://doi.org/10.1016/j.jenvman.2020.110868>
- [32] E. Apaydin-varol and E. Pütün, "Preparation and surface characterization of activated carbons from *Euphorbia rigida* by chemical activation with ZnCl₂, K₂CO₃, NaOH and H₃PO₄ Murat Kılıç," *Appl. Surf. Sci.*, vol. 261, pp. 247-254, 2012, <https://doi.org/10.1016/j.apsusc.2012.07.155>
- [33] A. Heidari, H. Younesi, A. Rashidi, and A. Ghoreyshi, "Adsorptive removal of CO₂ on highly microporous activated carbons prepared from *Eucalyptus camaldulensis* wood : Effect of chemical activation," *J. Taiwan Inst. Chem. Eng.*, vol. 45, no. 2, pp. 579-588, 2014, <https://doi.org/10.1016/j.jtice.2013.06.007>

- [34] K. S. O. and O. D. R. Olawale, "Characterization of optimized activated carbon production from soyabeans pod Characterization of optimized activated carbon production from soyabeans pod," in *Earth and Environmental Science*, 2025. <https://doi.org/10.1088/1755-1315/445/1/012054>
- [35] H. Nassar, A. Zyoud, A. El-hamouz, R. Tanbour, and N. Halayqa, "Aqueous nitrate ion adsorption / desorption by olive solid waste-based carbon activated using ZnCl_2 ," *Sustain. Chem. Pharm.*, vol. 18, 2020, <https://doi.org/10.1016/j.scp.2020.100335>
- [36] T. S. Tessema, A. T. Adugna, and M. Kamaraj, "Removal of Pb (II) from Synthetic Solution and Paint Industry Wastewater Using Activated Carbon Derived from African Arrowroot (*Canna indica*) Stem," *Adv. Mater. Sci. Eng.*, vol. 2020, 2020, <https://doi.org/10.1155/2020/8857451>
- [37] G. Yirdaw, A. Dessie, L. Bogale, and M. Genet, "Application of Noug (*Guizotia abyssinica* cass.) stalk activated carbon for the removal of lead (II) ions from aqueous solutions," *Heliyon*, vol. 10, no. 9, 2024, <https://doi.org/10.1016/j.heliyon.2024.e30532>